The Canadian Mineralogist
Vol. 37, pp. 1211-1227 (1999)

THE ORIGIN OF THE ATSHAN TALC DEPOSIT IN THE HAMATA AREA, EASTERN DESERT, EGYPT: A GEOCHEMICAL AND MINERALOGICAL STUDY

EVA S. SCHANDL[§]

Department of Geology, University of Toronto, 22 Russell Street, Toronto, Ontario M5S 3B1, Canada

NADIA A. SHARARA

Department of Geology, Faculty of Science, Assiut University, Assiut, 71516, Egypt

MICHAEL P. GORTON

Department of Geology, University of Toronto, 22 Russell Street, Toronto, Ontario M5S 3B1, Canada

Abstract

The Atshan talc mine is one of several talc deposits in the Hamata area of southeastern Egypt. Our detailed geochemical and mineralogical investigation suggests that precursors to the talc orebodies were impure dolomitic limestones locally intercalated with clastic sediments. The extremely low concentrations of trace elements, including the *REE*, and the low and variable Al concentrations in these rocks are inconsistent with igneous protoliths. The magnesium needed to form the talc orebodies was derived from the breakdown of pre-existing carbonates. This mode of origin is comparable to that in other carbonate-hosted talc deposits on the global scale, such as the Rabenwald and Lassing deposits in Austria. Rocks at the Atshan mine have been subjected to at least two episodes of metamorphism, contact and regional. Mineral assemblages (a) enstatite + cordierite + hercynite (granulite facies) and (b) enstatite + clinopyroxene (pyroxene hornfels facies) probably crystallized during emplacement of the Reiidi grey granite (contact metamorphism), and represent relict high-temperature assemblages in the clastic fragments. Temperatures above 600°C are suggested for the enstatite–cordierite pair, and a minimum range of temperatures between 500° and 600°C was estimated for the pyroxene hornfels. The serpentine + talc + tremolite + chlorite assemblage replaced the carbonates during regional metamorphism and associated faulting and shearing. The maximum temperature for this mineral assemblage is limited to <500°C, and the $X(CO_2)$ of the fluid is limited to <0.2 by the ubiquitous presence of serpentine. Stable reactions in the system of $CaO - MgO - SiO_2 - H_2O - CO_2$ demonstrate that serpentine and tremolite at the Atshan deposit could have formed during prograde reactions, and talc, during retrograde reactions. Small lenses of massive and disseminated sulfide (pyrite, pyrrhotite, sphalerite, chalcopyrite) within the talc orebodies may represent sulfide segregation in the original sediments prior to metamorphism. Some of the pyrite and pyrrhotite grains are fragmented and rimmed by talc, suggesting that they were present prior to talc mineralization. Chalcopyrite was probably remobilized, and it occurs along tremolite cleavages and fractures.

Keywords: Atshan deposit, talc, carbonate, sediments, serpentine, contact metamorphism, regional metamorphism, geochemistry, rare-earth elements, Eastern Desert, Egypt.

Sommaire

La mine de talc d'Atshan exploite un parmi plusieurs gisements de talc de la région de Hamata, dans le sud-est de l'Egypte. D'après nos études géochimiques et minéralogiques, les précurseurs du talc étaient des calcaires dolomitiques impurs, avec intercalations locales de détritus clastique. Les concentrations extrêmement faibles des éléments traces, y comprises les terres rares, et les teneurs faibles et variables en Al dans ces roches, montrent qu'elles ne pourraient pas avoir été dérivées d'un précurseur igné. Le magnésium nécessaire pour former le talc a été libéré par déstabilisation de carbonates pré-existants. Ce mode d'origine est comparable à ce qui est proposé pour les gisements de talc dans un encaissant carbonaté à l'échelle mondiale, par exemple à Rabenwald et Lassing en Autriche. Les roches de la mine Atshan ont subi les effets d'au moins deux épisodes de métamorphisme, un de contact et l'autre régional. Les assemblages (a) enstatite + cordierite + hercynite (faciès granulite) et (b) enstatite + clinopyroxène (faciès cornéennes à pyroxène) se seraient formés au cours de la mise en place du granite gris de Reiidi (métamorphisme de contact), et représenteraient des reliques d'assemblages de température élevée dans les fragments d'origine clastique. Une température supérieure à 600°C semble indiquée par l'assemblage enstatite–cordierite, et un intervalle minimum

§ *E-mail address*: schandl@zircon.geol.utoronto.ca

entre 500° et 600°C semble réaliste pour la cornéenne à pyroxène. L'assemblage serpentine + talc + trémolite + chlorite a remplacé les carbonates au cours d'un métamorphisme et une déformation régionales. La température maximale indiquée par cet assemblage serait moins de 500°C, et la composition de la phase fluide, en termes de $X(CO_2)$, ne peut dépasser 0.2 à cause de l'omniprésence de la serpentine. Les réactions stables dans le système $CaO - MgO - SiO_2 - H_2O - CO_2$ démontrent que serpentine et trémolite du gisement d'Atshan pourraient apparaître pendant les réactions progrades, et le talc, pendant les réactions rétrogrades. De petites lentilles de sulfures massifs et disséminés (pyrite, pyrrhotite, sphalérite, chalcopyrite) dans ces gisements pourraient être des ségrégations sulfurées dans les sédiments originels avant le métamorphisme. Dans certains cas, les grains de pyrite et de pyrrhotite sont brisés, et les fragments ont une bordure de talc, ce qui fait penser qu'ils précèdent la déposition du talc. La chalcopyrite a probablement été remobilisée, se trouvant maintenant dans les clivages et les fissures de la trémolite.

(Traduit par la Rédaction)

Mots-clés: gisement d'Atshan, talc, carbonate, sédiments, serpentine, métamorphisme de contact, métamorphisme régional, géochimie, terres rares, Désert Oriental, Egypte.

Introduction

The Atshan talc mine, in the Hamata area of the Eastern Desert, is the largest talc deposit in Egypt. There are thirty-five occurrences of talc in the Eastern Desert and Sinai of northeastern Egypt, and the main producers are the El Atshan and Darib mines. The Atshan mine, just as the other talc occurrences in the area, is associated with small lenses of sulfide (Hussein & El Sharkawi 1990), consisting of pyrite, sphalerite, chalcopyrite and galena. Although most of these sulfide occurrences are uneconomic, the Umm Samiuki deposit, located *ca.* 100 km southeast of El Atshan, is currently mined for Zn and Cu. The focus of the present study is a detailed investigation of the origin of talc mineralization at the Atshan mine and the metamorphic evolution of the deposit.

We investigated the mineralogy and geochemistry of a suite of twenty-one rock samples representative of the talc orebodies at the Atshan mine, and the mineralogy and geochemistry of volcanic rocks that host the deposit. The objectives of our study were (1) to determine the protolith of the talc-altered rocks using major, trace and rare-earth-element geochemistry, (2) to determine the source of Mg in the rocks, (3) to establish the metamorphic grade and the paragenetic sequence of alteration minerals at the deposit in order to develop a model for talc mineralization, and (4) to investigate the relationship of the Mg-rich rocks and the sulfides at the mine. Samples for the study were collected from the #1, #3 and #5 talc orebodies (Fig. 1).

Regional Setting

The Athsan talc mine is located in the Hamata area, 18 km west of the Red Sea. This area is considered to be part of the Arabian–Nubian Shield, which was first developed on an ocean arc complex (*cf.* Abdel-Rahman 1995, Vail 1985, Engel *et al.* 1980). The evolution of the complex took place between 600 and 1,000 m.y. ago, and the subduction-related emplacement of granitic plutons in eastern Egypt is bracketed between 550 and 880 Ma (Abdel-Rahman 1995). The presence of ophiolite suites and of remnants of island-arc-related volcanic and plutonic terranes suggests crustal accretion for the Arabian–Nubian Shield over the interval 950–550 Ma (Vail 1985). The talc deposits of the Hamata area occur within the Hamamid Group of the Shadli metavolcanic rocks, a sequence of mafic flows, andesites, dacites and pyroclastic rocks intercalated with some sediments (Fasfous 1992). The volcanic rocks were deposited within an island arc setting (Searle *et al.* 1976) and were later subjected to conditions of greenschist-facies metamorphism.

The Atshan mine was in operation intermittently from 1962 to 1992, and has an estimated reserve of about 60,000 tonnes of talc. The deposit is composed of several lensoid orebodies located along two distinct faults and within two shear zones (Fig. 1). The roughly N–S-trending shear zone is about 1300 m long and 200 m wide, whereas the E–W-trending shear is *ca.* 700 m long and 200 m wide. The largest orebody (No. 1) occurs within the E–W shear, and the second largest orebody (No. 5) occurs within the N–S shear zone. A large intrusive body, the Reiidi grey granite (composed of quartz diorite: Fasfous 1992) intrudes the volcanic rocks south of the mine, and localized stocks of the same occur within the mineralized zones.

Small lenses containing massive sulfides and disseminated sulfides (pyrite, pyrrhotite, sphalerite, lesser chalcopyrite and minor galena) occur in the two shear zones, and they are enclosed by the talc orebodies. The sulfide lenses are parallel to the shear zones, as well as to the banding in the host metavolcanic rocks (Zidan 1989). Although azurite, hematite and limonite-rich gossans outcrop at the surface, indicating supergene enrichment above the water table, most sulfides occur at depth.

Previous Work

The common association of talc with serpentine at the Atshan mine prompted some earlier investigators to suggest that the talc-rich rocks had mafic or ultramafic precursors (Nessim *et al.* 1954). More recent work of Abdel-Kader & Shalaby (1982), Fasfous *et al.* (1988),

and Fasfous (1992) demonstrated, however, that the low Cr and Ni concentrations in the Mg-rich rocks are inconsistent with a mafic or ultramafic protolith. Abdel-Kader & Shalaby (1982), Fasfous *et al.* (1988) and Fasfous (1992) suggested that the talc orebodies formed by Mg-metasomatism of pre-existing volcanic rocks. Fasfous (1992) also suggested that deposition of sulfide and talc in the area occurred during two separate (unrelated) fluid-circulation events. He attributed talc mineralization to "pyrometasomatism" and to the interaction of CO_2-rich fluids with volcanic rocks during the emplacement of igneous intrusions. Various hypotheses have been discussed in connection with the origin of sulfides at the Atshan mine and at similar talc deposits in the area. Early investigators suggested that the sulfides are epigenetic, and that they were introduced along faults and shear zones by hydrothermal fluids (Hume 1937, El Shazly & Afia 1958, Kovacik 1961, Mansour *et al.* 1962). More recently, investigators proposed that the sulfides in the talc-rich rocks represent VMS-type mineralization associated with Mg-metasomatism of the host rocks during felsic submarine volcanism (Hussein *et al.* 1977, Abdel Kader & Shalaby 1982, Rasmy *et al.* 1983). On the basis of a detailed petrological investigation, Zidan (1989) demonstrated that the sulfides in the metamorphosed talc-rich rocks at the Atshan mine are undeformed, suggesting an epigenetic origin. He conceded, however, that layering in some sulfides and the atoll texture displayed by some sulfides superficially resemble sedimentary textures. The grade and size of the (massive) sulfide occurrence at the Atshan talc mine have not been estimated, but the largest talc-associated Zn – Cu – Pb sulfide deposit, the Umm Samiuki deposit, has reserves of 132,000 tonnes of ore, grading 15.2% Zn, 1.15% Cu, and 1.1% Pb (Rasmy *et al.* 1983).

Analytical Techniques

Samples were analyzed for trace and rare-earth elements (*REE*) by instrumental neutron activation at the University of Toronto, using the techniques of Stix & Gorton (1992), and the chondrite-normalization factors (for the *REE*) of Barnes & Gorton (1984). Concentrations of major elements (on fused beads) and selected trace elements (on powder pellets) were determined by X-ray fluorescence, as well as by inductively coupled

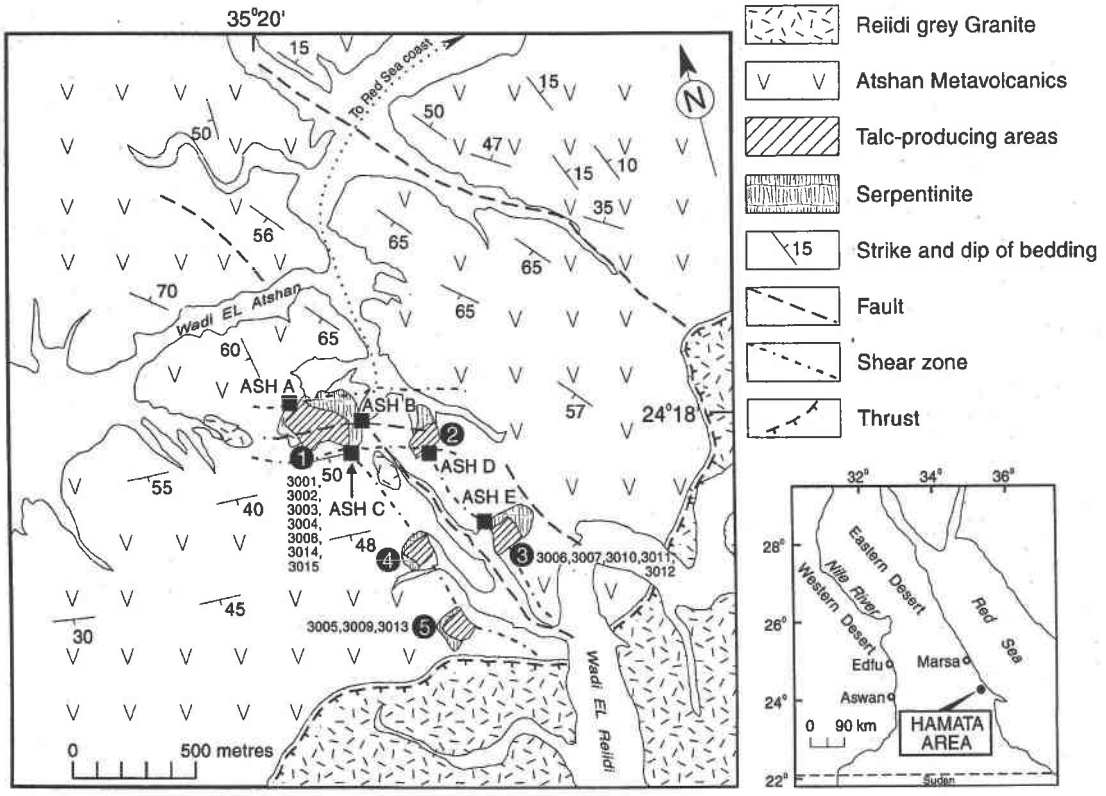

FIG. 1. Simplified geological and location map of the Atshan talc deposit (after Fasfous *et al.* 1988). Sample numbers are shown on the diagram, and the five orebodies are numbered.

plasma (ICP) analysis at Activation Laboratories, Ancaster, Ontario. The minerals were analyzed using CAMECA and ETEC electron microprobes at the Department of Geology, University of Toronto. Fluid-inclusion measurements were obtained on a LINKAM TH600 fluid inclusion stage at the Department of Geology, University of Toronto.

Mineralogy of Rocks from the Talc Orebodies

The mineral assemblages developed in individual samples are listed in the Appendix, and the composition of selected minerals is shown in Table 1. Excluding the suite of four igneous rocks, four distinct alteration assemblages were identified at the Atshan talc mine: (1) dolomite + serpentine ± talc, (2) talc + tremolite + carbonate, (3) orthopyroxene + clinopyroxene ± talc ± cordierite ± olivine ± serpentine, and (4) orthopyroxene + cordierite + chlorite + spinel ± talc ± clinopyroxene. A trace amount of quartz is present in most rocks. In addition to the above assemblages, one rock consists of chlorite + magnetite + apatite. Talc occurs in variable proportions in the above assemblages, and it is invariably the final product of alteration, replacing tremolite, serpentine, and orthopyroxene. In the high-grade talc zones, in which talc predominates and carbonates and serpentine are minor phases, the paragenetic sequence of alteration is difficult to see. However, where the replacement of earlier minerals by talc is incomplete, the sequence of alteration can be readily identified.

Assemblage 1

Mineral assemblage 1 occurs in the least metasomatized rocks and consists predominantly of dolomite, serpentine and minor quartz. The serpentine is interstitial to dolomite, and it seems to replace grains of olivine (Fig. 2B), although mesh-texture lizardite, partly recrystallized to antigorite, also was identified in some rocks (Fig. 2C). The carbonates and serpentine are both relatively Fe-poor; fine-grained talc is a minor phase, and it crystallized at the expense of serpentine.

Assemblage 2

Mineral assemblage 2 is simple, as it consists predominantly of talc + tremolite + carbonate (relict dolomite and late calcite) ± serpentine ± chlorite. The most common mineral in this assemblage is talc (up to 80 vol. %). Tremolite can occur as coarse-grained crystals (up to 1 cm long) of prismatic habit, or as radiating aggregates (Fig. 2A). Most of the tremolite is partly or completely replaced by talc (pseudomorphic replacement). Some coarse-grained tremolite contains small, corroded relict inclusions of dolomite. There is a wide range in Al concentration in tremolite, from 0.5 to 5.9 wt% Al_2O_3 (Table 1).

Assemblages 3 and 4

Mineral assemblages 3 and 4 are more complex than 1 and 2. The secondary minerals represent pyroxene hornfels and granulite-facies assemblages (orthopyroxene + clinopyroxene, orthopyroxene + cordierite + hercynite), as well as minor greenschist-facies assemblages (serpentine + chlorite + clinopyroxene + talc), which are superimposed on the high-temperature minerals. Orthopyroxene is in textural equilibrium with clinopyroxene and minor cordierite (3010), and orthopyroxene is in equilibrium with and is commonly intergrown with cordierite (3001, ASH–B and ASH–C), implying their contemporaneous crystallization. All three minerals are partly replaced by fine-grained talc. Orthopyroxene occurs as large prismatic grains, as fine-grained granular aggregates intergrown with diopside, as prismatic, fan-shaped aggregates, and as lath-shaped aggregates intergrown with cordierite (Fig. 2D).

The chlorite-rich rock (ASH–D) consists of chlorite + magnetite + ilmenite + quartz + apatite. The subrounded shape of magnetite and apatite suggests a detrital origin for these minerals, and the relative abundance of abraded zircon in the rock is consistent with a sedimentary origin. Other rocks distinct from the above three groups are 3008, 3013 (diorite fragments) and 3009 (albitite vein). These igneous fragments and the albitite vein are partly replaced by amphibole, which in turn is partly replaced by talc. The last three rocks have the highest concentration of Au (300–600 ppb) in the suite of 21 samples analyzed.

The sulfides identified at the Atshan talc deposit include pyrrhotite, sphalerite, minor pyrite, chalcopyrite and galena. Pyrite and pyrrhotite represent the earliest sulfides. Pyrite occurs in subhedral to anhedral aggregates in the rock matrix, or as inclusions in pyrrhotite. Most grains of pyrrhotite are fractured and fragmented, and the fractures are filled by chalcopyrite or talc, or both. Chalcopyrite appears to be a late sulfide, as it commonly forms a rim on sphalerite and occurs as veinlets along cleavages in grains of lath-shaped tremolite (Fig. 2E). The most common minerals associated with chalcopyrite and sphalerite are relict carbonate, orthopyroxene and tremolite. As talc rims the sulfides, or lines the fractures in them, talc apparently postdated most sulfides.

Mineralogy of the Volcanic Rocks

Representative samples were collected from the volcanic rocks from the north side of the no. 1 and 2 orebodies at the talc mine (andesite and basalt). The least-altered volcanic rock is andesite, consisting of euhedral, zoned plagioclase phenocrysts (An_{35}) and hornblende phenocrysts set in a matrix of fine-grained

TABLE 1. SELECTED RESULTS OF ELECTRON-MICROPROBE ANALYSES OF MINERALS FROM THE ATSHAN MINE, EASTERN DESERT, EGYPT

Sample	ASH –B	ASH –B	ASH –B	3002	3001	3010	3010	ASH –C	3004	3004	3004	3015
Mineral	Opx	Opx	Opx	Opx	Opx	Opx	Opx	Opx	Tr	Tr	Tr	Tr
SiO_2 wt.%	52.51	53.03	52.85	57.45	53.36	48.08	52.00	55.69	59.42	58.26	58.18	56.52
TiO_2	0.30	0.06	0.02	0.05	0.07	0.00	0.00	0.00	0.07	0.13	0.11	0.02
Al_2O_3	3.87	2.89	2.93	0.22	5.42	11.34	5.22	6.55	0.41	2.70	2.40	5.92
FeO*	11.91	12.41	13.28	1.40	9.10	1.07	9.08	5.31	0.41	0.65	0.63	0.00
MnO	0.26	0.22	0.23	0.02	0.15	0.00	0.00	0.00	0.36	0.11	0.09	0.00
MgO	29.20	29.01	28.44	40.12	32.59	35.63	33.10	32.18	24.11	24.00	23.87	23.10
CaO	0.19	0.19	0.19	0.03	0.08	2.90	0.00	0.00	13.77	13.17	13.61	13.23
Total	98.24	97.81	97.94	99.29	100.77	99.02	99.40	99.73	98.55	99.02	98.89	98.79
Si *apfu*	1.896	1.900	1.924	1.954	1.854	1.657	1.834	1.905	7.962	7.711	7.804	7.560
^{IV}Al	0.104	0.100	0.075	0.009	0.146	0.343	0.166	0.098	0.038	0.289	1.960	0.440
^{VI}Al	0.061	0.027	0.050	0.000	0.076	0.118	0.051	0.169	0.059	0.133	0.099	0.364
Ti	0.008	0.002	0.001	0.003	0.001	0.000	0.000	0.000	0.007	0.132	0.011	0.002
Fe	0.359	0.371	0.404	0.040	0.265	0.030	0.268	0.152	0.047	0.065	0.065	0.000
Mn	0.007	0.007	0.006	0.000	0.004	0.000	0.000	0.000	0.033	0.011	0.009	0.000
Mg	1.571	1.620	1.544	2.033	1.688	1.831	1.739	1.641	4.835	4.739	4.773	4.600
Ca	0.007	0.008	0.007	0.001	0.000	0.134	0.000	0.000	1.984	1.870	1.956	1.894

Sample	ASH –C	ASH –C	ASH –C	ASH –C	ASH –B	3002	ASH –E	3012	3012	3012	3010	3002	3004
Mineral	Ol	Ol	Crd	Crd	Crd	Srp	Srp	Srp	Srp	Srp	Srp	Tlc	Tlc
SiO_2 wt.%	41.70	41.52	49.90	50.52	50.26	42.14	43.69	44.50	45.10	44.70	44.75	63.51	64.24
Al_2O_3	0.00	0.00	36.18	34.88	34.63	0.00	0.90	0.04	0.07	0.70	0.00	2.90	2.80
FeO*	5.32	5.45	0.60	0.65	1.75	3.82	0.86	0.46	0.80	0.81	1.05	1.17	0.00
MgO	52.56	52.59	13.47	13.34	12.79	42.10	43.69	41.67	41.34	41.56	42.21	31.51	31.56
Total	99.58	99.56	100.15	99.39	99.43	88.06	89.14	86.67	87.31	87.77	88.01	99.09	98.60
X_{Mg}	0.96	0.95											
Si *apfu*	1.001	1.001	4.872	4.966	4.965	1.964	1.976	2.056	2.070	2.053	2.018	7.759	7.831
^{IV}Al	0.000	0.000	1.128	1.034	1.035	0.000	0.024	0.000	0.000	0.000	0.000	0.241	0.169
^{VI}Al	0.000	0.000	3.036	3.006	2.993	0.000	0.023	0.001	0.001	0.025	0.000	0.176	0.234
Fe	0.107	1.110	0.049	0.053	0.145	0.149	0.326	0.018	0.031	0.030	0.127	0.120	0.000
Mg	1.885	1.889	1.960	1.954	1.883	2.924	2.944	2.869	2.828	2.826	2.837	5.737	5.733

Sample	3010	3010	3007	3001	3010	ASH –D	ASH –C	ASH –E	ASH –E	3012	3007	ASH –E
Mineral	Di	Di	Chl	Chl	Chl	Chl	Phl	Dol	Dol	Dol	Cal	Dol
SiO_2 wt.%	55.41	53.39	30.78	30.15	31.94	28.92	43.17					
TiO_2	0.00	0.00	0.07	0.08	0.00	0.07	2.39					
Al_2O_3	0.00	0.64	21.13	20.51	18.24	20.63	13.91					
FeO*	0.28	0.37	1.56	4.62	0.80	10.88	2.56	0.10	0.00	0.11	0.00	0.00
MnO	0.00	0.00	0.07	0.04	0.00	0.17	0.00	1.49	1.05	1.07	0.16	1.09
MgO	17.87	18.07	33.89	31.95	36.74	27.19	27.11	19.55	20.91	18.08	0.00	19.81
CaO	26.01	26.09	0.00	0.00	0.00	0.00	0.00	33.00	32.86	34.37	55.23	33.85
K_2O							8.37					
Total	99.57	98.56	87.65	87.35	87.72	87.86	97.51	54.14	54.82	53.63	55.39	54.75
Si *apfu*	2.008	1.964	5.711	5.695	5.901	5.618	5.847					
^{IV}Al	0.000	0.027	2.289	2.305	2.099	2.382	2.153					
^{VI}Al	0.000	0.000	2.334	2.263	2.073	2.343	0.069					
Ti	0.000	0.000	0.010	0.023	0.000	0.100	0.243					
Fe	0.009	0.011	0.243	0.730	0.123	1.767	0.000	0.003	0.000	0.003	0.000	0.000
Mn	0.000	0.000	0.009	0.006	0.000	0.023	0.290	0.031	0.026	0.023	0.004	0.028
Mg	0.964	0.991	9.372	8.996	10.116	7.867	5.473	0.888	0.927	0.834	0.000	0.885
Ca	1.010	1.028	0.000	0.000	0.000	0.000	0.000	1.077	1.047	1.140	1.996	1.087
K							1.447					

* Total Fe expressed as FeO. Symbols: Opx: orthopyroxene, Tr: tremolite, Ol: olivine, Crd: cordierite, Srp: serpentine, Tlc: talc, Di: diopside, Chl: chlorite, Phl: phlogopite, Dol: dolomite, Cal: calcite.

** Structural formulae are calculated for each mineral on the basis of the appropriate number of atoms of oxygen: opx: 6, tr: 23, ol: 4, crd: 18, srp: 7, tlc: 22, di: 6, chl: 28, phl: 22, dol: 6, cal: 6.

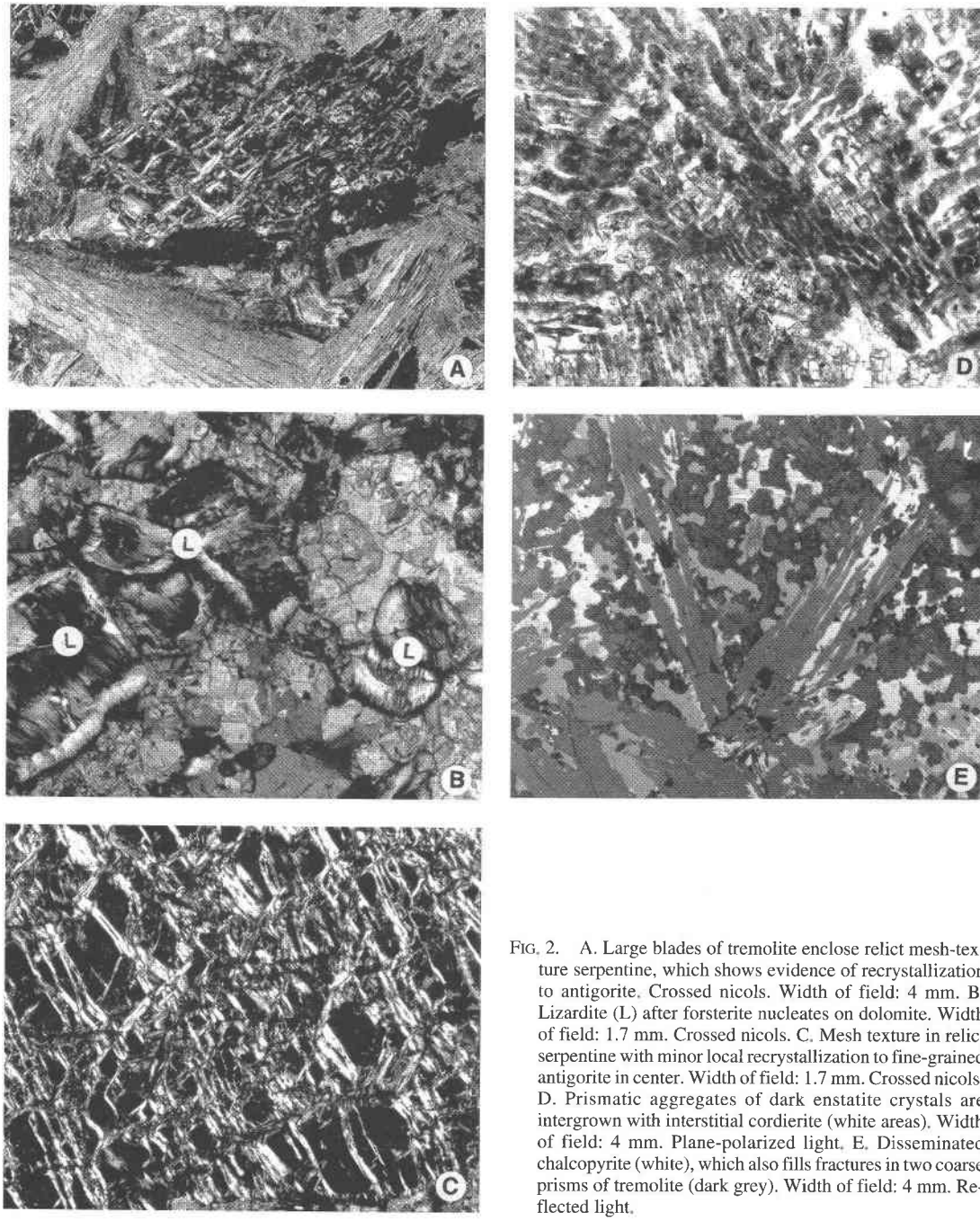

FIG. 2. A. Large blades of tremolite enclose relict mesh-texture serpentine, which shows evidence of recrystallization to antigorite. Crossed nicols. Width of field: 4 mm. B. Lizardite (L) after forsterite nucleates on dolomite. Width of field: 1.7 mm. Crossed nicols. C. Mesh texture in relict serpentine with minor local recrystallization to fine-grained antigorite in center. Width of field: 1.7 mm. Crossed nicols. D. Prismatic aggregates of dark enstatite crystals are intergrown with interstitial cordierite (white areas). Width of field: 4 mm. Plane-polarized light. E. Disseminated chalcopyrite (white), which also fills fractures in two coarse prisms of tremolite (dark grey). Width of field: 4 mm. Reflected light.

amphibole, plagioclase and magnetite. The plagioclase phenocrysts are partly altered to clinozoisite, and some amphibole phenocrysts are partly recrystallized to blue-green actinolite. The mafic rocks are extensively converted to amphibolite; plagioclase is replaced by a mixture of fine-grained actinolite and clinozoisite, and hornblende is replaced by actinolite. Fine-grained Ti-rich magnetite in the matrix is partly replaced by "leucoxene" and hematite. The abundance of Ti-rich magnetite in one sample of basalt suggests high con-

centrations of Ti in the rock. Chlorite, although present, is relatively rare in the volcanic rocks.

Fluid Inclusions

Four small (3 μm) primary fluid inclusions were identified (sample ASH–E) in lizardite. This rock consists predominantly of carbonate and serpentine. Fluid inclusions are rare in serpentine, and because of their small size, reliable measurements of freezing temperature could not be obtained; thus the salinity of the fluid was not determined. The homogenization temperature (T_h), measured on all four inclusions, yielded a relatively narrow range of 280° to 310°C.

Geochemistry

Concentrations of major, trace and rare-earth elements in seventeen samples from the talc orebodies and four from the volcanic suite are shown in Table 2.

Rocks from the talc orebodies

Rocks from the ore zone have variable and very low concentrations of trace and *REE* (Table 2). As incompatible trace elements such as Ta, Hf, Zr, and Th are inert under most geological conditions (Schandl *et al.* 1995, 1999, Gorton *et al.* 1999), the low concentrations cannot be due to mobilization during metamorphism. The low concentrations of Al, Ta, Hf, Zr, Th and *REE* are inconsistent with a felsic igneous protolith, whereas the low concentrations of Cr, Ni, and Co concentrations are inconsistent a mafic igneous protolith. It is noteworthy that out of the seventeen rocks, eleven contain less than 3 wt.% Al_2O_3, four contain 4–8 wt.% Al_2O_3, and only three rocks contain more than 10 wt.% Al_2O_3. The compositional spectrum suggests that the rocks consist of detrital material (sediments) diluted by trace-element-poor components such as carbonate and quartz. The relatively high level of Hf (up to 3.2 ppm), coupled with low concentrations of Ni, Cr and Co in some samples,

TABLE 2. COMPOSITION OF ROCKS FROM THE HAMATA TALC DEPOSIT, EASTERN DESERT, EGYPT

Sample	ASH –A	ASH –B	ASH –C	ASH –E	3001	3002	3003	3004	3006	3007	3008	3009	3010	3011	3012	3013	3015	3016	3017	3018	3019
SiO_2 wt.%		33.09	43.24	16.17	54.51	54.16	53.23	54.60	63.05	42.02	54.64	55.33	48.40	26.87	13.59	65.91	55.90	50.50	50.49	53.89	62.94
TiO_2		0.07	0.20	<0.10	0.12	0.05	0.09	0.22	0.02	0.12	0.28	0.23	0.05	0.02	0.01	0.42	0.07	0.63	2.58	0.66	0.64
Al_2O_3		11.95	13.99	0.38	8.34	1.37	2.34	3.16	1.03	4.63	8.70	4.31	2.53	0.59	0.36	13.11	2.48	18.63	14.84	16.65	16.69
Fe_2O_3*	3.49	22.82	7.36	0.42	2.79	1.93	1.07	1.00	0.21	1.79	11.63	8.53	0.89	1.06	0.45	2.93	0.40	12.10	12.93	13.25	4.89
MnO		0.10	0.11	0.95	0.08	0.07	0.06	0.11	0.04	0.12	0.27	0.12	0.14	0.12	1.07	0.09	0.09	0.19	0.18	0.20	0.09
MgO		22.61	28.96	27.69	29.48	34.11	34.05	26.13	30.89	32.15	16.51	23.93	27.24	24.25	26.08	5.50	27.99	3.97	4.73	3.92	3.10
CaO		1.34	0.58	21.73	0.44	0.48	0.32	9.17	0.34	8.52	2.29	1.73	12.53	20.71	22.25	2.48	7.55	10.71	6.15	8.83	6.05
Na_2O	0.08	0.10	0.14	0.03	0.23	0.11	0.18	0.38	0.48	0.09	1.16	0.74	0.32	0.15	0.04	5.00	0.37	1.13	3.70	1.22	3.89
K_2O		0.12	0.18	0.03	0.40	0.03	0.07	0.07	0.01	0.01	0.17	0.12	0.01	0.01	0.01	1.07	0.01	0.21	1.67	0.30	0.37
P_2O_5		0.89	0.33	0.11	0.20	<0.01	0.03	0.15	0.03	0.02	0.06	0.04	0.14	0.10	0.35	0.19	0.06	0.04	0.52	0.02	0.12
LOI		7.15	5.57	33.25	4.09	7.95	8.74	4.42	4.69	11.19	4.66	4.79	7.28	24.36	34.96	2.25	4.24	0.69	3.05	0.94	1.72
Total		100.24	100.66	100.77	100.67	100.25	100.17	99.41	100.78	100.64	100.37	99.84	99.49	98.23	99.14	98.95	99.14	98.81	100.84	99.86	100.50
Zr ppm		39	117	14	63	18	38	28	8	34	26	19	14	10	4	97	14	22	259	19	81
Y		15	36	10	19	8	8	5	1	10	9	5	7	8	8	17	1	9	31	10	12
Sr	4	13	7	30	14	7	6	18	11	5	79	40	12	21	24	272	13	183	359	164	467
La	2.156	2.923	3.311	1.503	1.682	0.154	0.323	1.390	0.717	1.084	2.143	1.435	1.154	2.321	1.648	9.493	1.187	0.877	38.330	1.518	6.818
Ce	7.722	8.465	9.992	2.778	4.590	0.919	1.579	2.910	1.443	3.119	5.100	3.400	4.207	3.448	3.668	20.526	2.839	2.400	94.000	5.100	18.500
Nd	4.448	6.426	8.561	2.142	4.575	0.320	0.817	2.419	0.617	3.100	3.930	2.452	2.376	2.495	2.608	10.330	1.251	n.d.	39.890	3.372	8.108
Sm	1.606	2.734	3.019	0.522	1.549	0.128	0.470	0.527	0.143	0.898	1.108	0.657	0.675	0.672	0.769	3.143	0.248	0.817	9.412	1.084	2.387
Eu	0.440	1.162	0.699	0.253	0.370	0.051	0.151	0.242	0.091	0.375	0.449	0.235	0.296	0.282	0.302	0.676	0.307	0.390	2.500	0.500	0.800
Tb	0.508	0.417	0.680	0.121	0.374	0.056	0.127	0.116	0.047	0.244	0.223	0.144	0.187	0.156	0.152	0.422	0.058	0.200	1.160	0.280	0.370
Yb	3.513	1.455	4.950	0.336	2.328	0.340	0.717	0.480	0.087	1.149	1.025	0.794	0.682	0.780	0.408	1.632	0.217	1.127	2.910	1.261	1.278
Lu	0.493	0.229	0.762	0.056	0.367	0.057	0.111	0.081	0.024	0.196	0.169	0.145	0.108	0.131	0.057	0.250	0.035	0.194	0.412	0.210	0.187
$La/Yb_{(N)}$	0.4	1.3	0.4	3.0	0.4	0.3	0.3	1.9	5.5	0.6	1.4	1.0	1.1	2.2	2.7	3.8	3.8	0.5	8.7	0.8	3.8
Hf	2.981	0.963	3.191	0.186	1.843	0.352	0.601	0.630	0.150	0.859	1.556	1.306	0.697	0.101	0.186	3.554	0.447	0.510	6.400	0.710	2.410
Ta	0.130	0.024	0.127	0.023	0.056	0.026	0.050	0.049	0.021	0.051	0.038	0.043	0.039	0.007	0.021	0.230	0.045	0.030	2.740	0.080	0.140
Th	1.114	0.363	0.653	0.135	0.520	0.094	0.146	0.330	0.194	0.160	1.561	0.630	0.334	0.257	0.042	1.015	0.209	0.150	3.830	0.180	1.220
Sc	11.30	8.75	18.25	0.78	8.65	2.09	3.72	2.50	0.20	4.51	24.80	23.60	1.86	0.75	0.92	15.73	0.19	50.00	20.02	49.20	13.50
Cr	4	5	1	2	3	3	2	4	3	4	41	63	7	3	8	25	4	27	61	14	44
Ni	7	9	2	0	3	9	21	20	22	7	104	37	50	15	14	21	25	n.d.	n.d.	n.d.	n.d.
Co	4	2	1	0	1	1	1	1	1	2	46	29	2	3	2	6	2	36.7	41.12	34.63	17.6
Zn	950	230	240	1810	250	2100	850	1600	2460	520	2290	2600	3520	2300	1980	1570	1130	n.d.	n.d.	n.d.	n.d.
Ag	n.d.	n.d.	n.d.	n.d.	n.d.	n.d.	n.d.	n.d.	n.d.	n.d.	n.d.	n.d.	n.d.	n.d.	n.d.	117	n.d.	n.d.	n.d.	n.d.	n.d.
Au ppb	30	83	50	41	24	29	14	27	9	15	597	460	77	154	30	315	35	34	42	75	83

Fe_2O_3*: Fe total expressed as Fe_2O_3. n.d.: not detected, blank: not analyzed. Samples 3016 – 3019 are of volcanic origin.

imply that the detrital component is unlikely to have been derived from mafic rocks.

On a chondrite-normalized diagram (Fig. 3A), the rocks have a narrow range in $La/Yb_{(N)}$ values (<1–5), and a wide range in *REE* concentrations. The comparable shape of the *REE* patterns suggests that the sediments (carbonate and clastic) were probably derived from a common source, whereas the range in concentrations suggests variable dilution by a *REE*-poor component. Although the rocks also show a large scatter on a Ta/Yb – Th/Yb diagram (Fig. 4), they all plot in the area occupied by arc material (island-arc tholeiites and active continental margins).

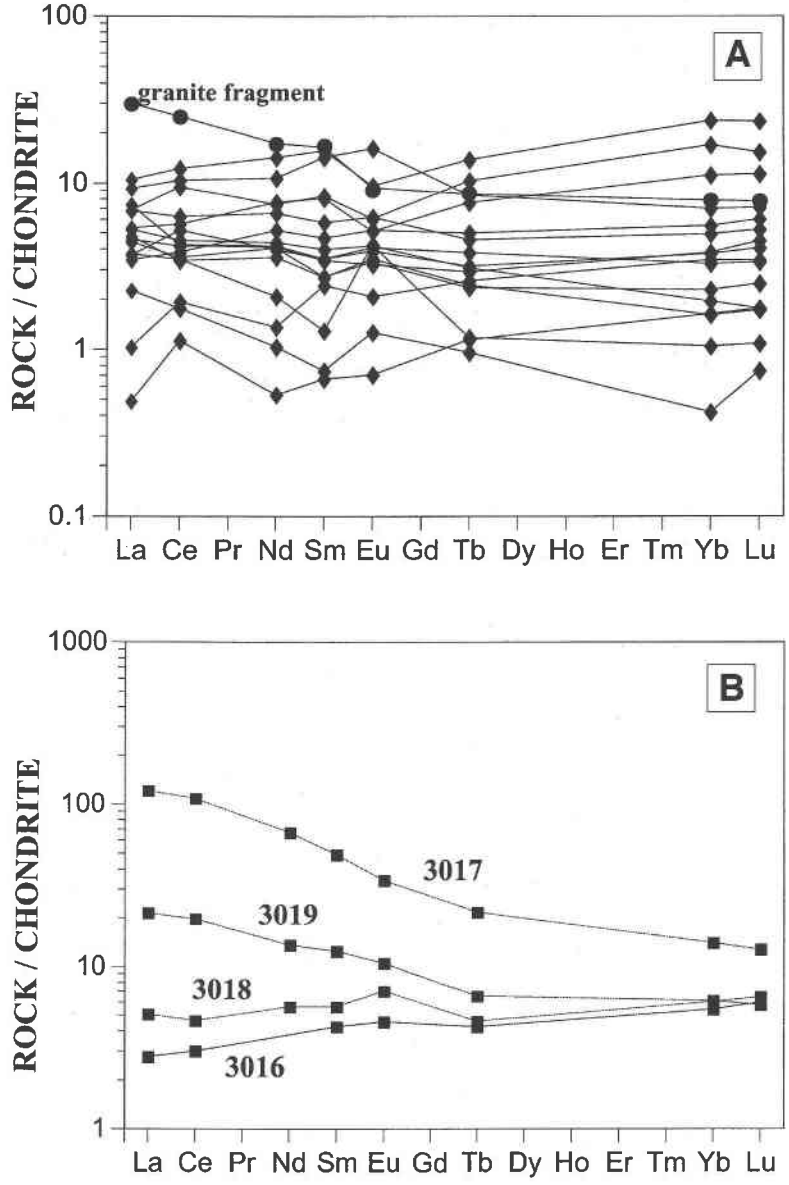

FIG. 3. A. Chondrite-normalized plot of the *REE* abundances in a suite of seventeen rocks from the talc orebodies. B. Chondrite-normalized *REE* plot of the volcanic rocks from the mine.

Anomalous concentrations of Au and Ag were found in two samples identified as diorite fragments (315–597 ppb Au and 117 ppm Ag), and in a tremolite-rich rock that is cross-cut by a vein of coarse-grained albitite (460 ppb Au). To our knowledge, this is the first time that elevated gold and silver concentrations have been reported from the Atshan talc deposit. Although the source of Au and Ag is not known at present, their association with intrusive rocks and the albitite vein suggests a possible relationship between igneous activity and the enrichment in precious metals.

Geochemistry of the volcanic rocks

The suite of volcanic rocks collected at the mine includes three metabasalts and one meta-andesite. One basaltic rock (3017) has high concentrations of TiO_2, Zr, Hf, Ta and the light rare-earth elements (*LREE*) (Fig. 3B), and plots on the upper part of the area defined for within-plate basalts (WPB) on the Ta/Yb – Th/Yb diagram (Fig. 4). The two samples of primitive basalt (3016, 3018) have low concentrations of TiO_2, Zr, Hf and Ta, they are slightly depleted in *LREE* (Fig. 3B), and plot in the island-arc tholeiite (IAT) area on Figure 4. The andesite (3019) is slightly enriched in *LREE* with respect to the tholeiites (Fig. 3B), and it plots with magmas formed at active continental margins (ACM) in Figure 4.

Discussion

Geochemistry

A striking feature of the rocks that host the Atshan talc deposit is the low and variable concentrations of "immobile" elements, such as Hf, Ta, Th, Zr, and Al. As these elements are relatively immobile during metamorphism and hydrothermal alteration (*cf.* Schandl *et*

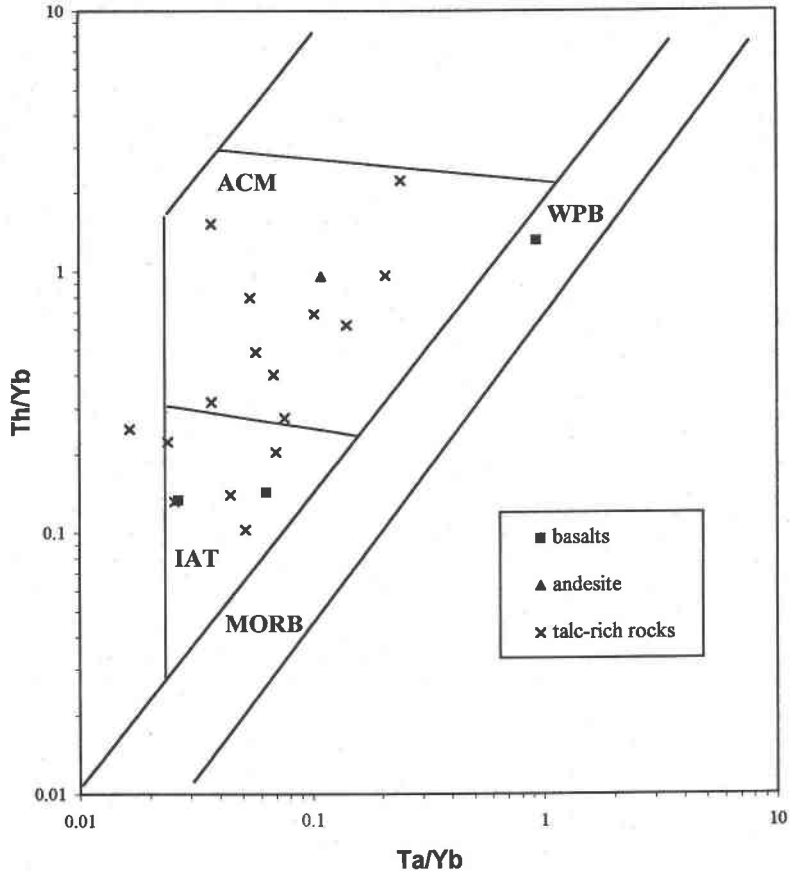

FIG. 4. Ta/Yb – Th/Yb plot. ACM: active continental margins, WPB: within-plate basalts, IAT: island-arc tholeiites, and MORB: mid-ocean ridge basalts (after Pearce 1983).

al. 1995), the values must reflect the composition of the original rocks. The low concentrations of Hf, Ta and Th in 14 of the 17 rocks analyzed, and the very low Al_2O_3 and Zr concentrations, are inconsistent with igneous protoliths. Thus we do not agree with previous investigators who suggested that the talc orebodies represent Mg-metasomatized volcanic rocks (*cf.* Abdel Kader & Shalaby 1982, Fasfous 1992) or pre-existing Mg-silicates (tremolite) CO_2-metasomatized during "pyrometasomatism" (Fasfous 1992). The trace- and major-element data pertaining to rocks from various talc deposits in the Hamata area that were presented by Fasfous (1992) in fact support our conclusions, that the protolith of these rocks are sediments consisting predominantly of carbonate beds and a minor clastic component. His magnesium-rich rocks, with concentrations in the range of 23–38 wt.% MgO, have extremely low Zr and Al_2O_3 concentrations (Zr in the range 24–50 ppm, Al_2O_3 in the range 0.38–1.24 wt.%), and very low Cr and Ni concentrations (<15 ppm). These values indicate that the talc orebodies could not have formed by Mg-metasomatism of felsic or any other type of igneous rocks.

The very low concentrations of trace and rare-earth elements and the low and variable concentration of Al_2O_3 in the altered rocks of the Atshan talc deposit, and the abundance of carbonates, suggest that the massive talc orebodies probably formed as replacement of dolomitic, siliceous, impure limestones that contained fragments of clastic sediments. This conclusion is supported by field observations. Fasfous (1992) described massive white carbonates within the talc deposit, but suggested that their crystallization was more or less contemporaneous with talc mineralization during "pyrometasomatism". We propose that the carbonates represent relict beds of siliceous dolomite (or possibly magnesite) that were deposited prior to intrusion of the Reiidi grey granite; thus they predated talc mineralization. Petrographic observations suggest that serpentine nucleated on carbonates in the almost monomineralic carbonate-rich rocks, and the serpentine clots commonly have olivine forms, suggesting that olivine was an intermediate (but evidently metastable) phase prior to serpentinization. Although present, free quartz is a relatively minor component of these rocks. To our knowledge, carbonate beds of sedimentary origin have not previously been identified at the Atshan mine and in the Hamata area.

Two of the basalt samples, 3016 and 3018, lie in the field of island-arc tholeiites in Figure 4. Their *REE* patterns are low, with a slight positive slope; they have low Mg and high Al concentrations, as is typical of arc tholeiites. Although the andesite, 3019, plots in the field of active continental margin field magmas, it also has the characteristic low *REE* concentrations and slight *LREE* enrichment typical of arc tholeiites, suggesting that the andesite is part of the tholeiite suite. The geochemistry of the basalts and andesite confirms the work of previous investigators who identified the presence of island-arc rocks in the Eastern Desert (*cf.* Abdel-Rahman 1995, Engel *et al.* 1980). As arc tholeiites are typical of intra-oceanic arcs, their presence confirms an oceanic depositional environment for the rocks in the area. It is noteworthy that the composition of the seventeen rocks from the talc orebodies also plots on the arc sections of the Ta/Yb – Th/Yb diagram (Fig. 4), suggesting that the detrital component also was derived from an arc environment.

Sample 3017 is geochemically different from the tholeiites and plots in the within-plate basalt field (WPB) in Figure 4. Incompatible elements and element ratios are more enriched than in continental tholeiites, and although not nepheline-normative, this rock appears to have a closer affinity with alkaline basalts. This may be a high-level intrusive rock, the age of which is uncertain. Thus, it is not possible to evaluate its tectonic significance.

Mineralogy and phase relationships

The talc orebodies at the Atshan mine locally contain relict carbonate-rich patches in which serpentine nucleated (*via* olivine) on carbonate. Textural evidence suggests that talc was the final product of alteration in rocks consisting of tremolite, serpentine and carbonate. This is consistent with observations of Fasfous (1992), who suggested that talc at the mine commonly formed as replacement after tremolite and serpentine. That clastic sediments were locally interbedded with the original limestones is evident from the presence of Al-rich minerals such as cordierite and hercynite, and by the wide range of Al concentrations in the rocks, from 0.4 wt% (3012) to 14 wt% (ASH–C) Al_2O_3. Thus we suggest that the Mg-rich silicates such as talc, serpentine, and tremolite were not produced by magnesium metasomatism, but by the progressive breakdown of pre-existing Mg-rich carbonates during decarbonation reactions of impure carbonate beds. SiO_2 (to form the silicates) was probably derived from the dissolution of chert beds or from siliceous, clastic sediments.

The complex mineral assemblages at the Atshan talc deposit reflect the bulk-rock composition and the composition of metamorphic fluids. Rocks with low concentrations of Al (0.5–4.5 wt.% Al_2O_3) mostly contain dolomite–calcite, talc, tremolite, and serpentine ± diopside, whereas in rocks with relatively high concentrations of Al (8–14 wt.% Al_2O_3), the common minerals are orthopyroxene, cordierite, chlorite + hercynite (± olivine ± serpentine ± talc ± tremolite). The localized occurrence of fragments containing the assemblages cordierite – orthopyroxene – hercynite and orthopyroxene – clinopyroxene within the talc orebodies suggests that the rocks at one time must have been subjected to upper amphibolite to granulite-facies metamorphism (*cf.* Ballèvre *et al.* 1997, Guiraud *et al.* 1996, Harris & Holland 1984, Hoffer & Grant 1980). These relict, high-temperature minerals, which occur within

the greenschist-facies assemblage in the talc orebodies (talc – tremolite – serpentine ± carbonate), also contain minor talc Å serpentine Å olivine. The alteration assemblages in the volcanic rocks are also consistent with greenschist-facies metamorphism in the area. Evidently, the sediments at the Atshan talc deposit were subjected to more than one metamorphic episode. The orthopyroxene – cordierite ± hercynite assemblage (ASH–B, ASH–C, 3001), and the orthopyroxene – clinopyroxene assemblage (3010) in the no.1 and no. 3 orebodies, respectively, represent a high-temperature event, whereas the serpentine – tremolite – talc assemblage represents a superimposed, lower-temperature event associated with carbonate replacement. In both rock types (carbonates and clastic sediments), talc was the last metamorphic mineral to crystallize. Figure 5 demonstrates some possible reactions in the evolution of the serpentine – tremolite – talc assemblages at the Atshan talc mine. These reactions are discussed in the following section.

Experimental investigations of the system CaO – MgO – SiO_2 – CO_2 – H_2O suggest that mineral assemblages consisting of carbonate, olivine, tremolite, talc and serpentine crystallize in the presence of fluids having variable ratios of H_2O and CO_2 (*cf.* Trommsdorff & Evans 1977, Skippen 1974). Depending on temperature and fluid composition [$X(CO_2)$], there are several possible paths; serpentine-absent reactions occur in the CO_2-rich part of a T–$X(CO_2)$ diagram, whereas serpentine-present reactions occur on the H_2O-rich part of the diagram (*cf.* Trommsdorff & Evans 1977). The replacement of carbonates by olivine and subsequently by serpentine is facilitated by fluids with $X(CO_2)$ less than 0.20 at <500°C (and 2 kbar pressure), whereas the crystallization of tremolite is facilitated by fluids having a

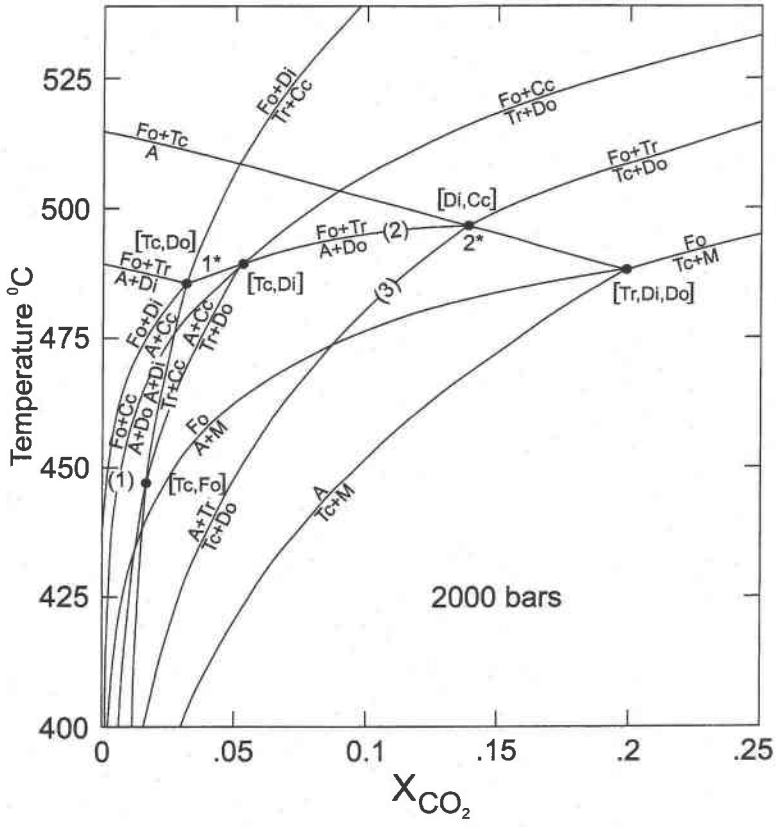

FIG. 5. Stable reactions in the system of CaO–MgO–SiO_2–H_2O–CO_2 are shown on a T *versus* $X(CO_2)$ diagram at a total pressure of 2000 bars (after Trommsdorff & Evans 1977). Univariant curves 1, 2 and 3 represent reactions suggested for the evolution of the serpentine – tremolite – talc assemblage at the Atshan talc mine. Symbols in the diagram (from Trommsdorff & Evans 1977) are the same as used in the Appendix, except that A, Cc, Tc and M represent antigorite, calcite, talc and magnesite, respectively.

wider range in $X(CO_2)$ (<0.05–0.9) and temperature (400°–625°C) (Trommsdorff & Evans 1977, Skippen 1974). As serpentine was identified in most rocks at the Atshan deposit, reactions leading to the crystallization of talc should occur in the low-$X(CO_2)$ part of such a diagram (Fig. 5). Whereas the temperature of crystallization of the early orthopyroxene–cordierite assemblage must have been above 600°C, the temperature of crystallization of the assemblage containing serpentine must have occurred at <500°C. It is apparent from Figure 5 that the stability of serpentine is limited not only by temperature, but also by $X(CO_2)$ of the fluid. Serpentine becomes unstable if $X(CO_2)$ in the fluid is less than 0.2, and it then recrystallizes to talc + carbonate (Fig. 5). The experimental work of Johannes (1969) and Greenwood (1967) demonstrates that the breakdown of serpentine to quartz + magnesite and talc + magnesite occurs at *ca.* 450°C and in the presence of fluid with a low value of $X(CO_2)$. Mineral assemblages formed by these reactions have been documented in ultramafic rocks at several locations in the Abitibi greenstone belt by Schandl (1989), Schandl & Wicks (1991, 1993), and Schandl & Naldrett (1992), among others, and the fluid temperature was determined from fluid inclusions by microthermometry. As massive serpentinite partly envelops the talc orebodies at the Atshan mine, reactions above 500°C and fluids of high values of $X(CO_2)$ would be inconsistent with the experimental results. Thus the mineral assemblage serpentine – tremolite – talc at the Atshan deposit probably crystallized by reactions shown on the univariant curves in the low-$X(CO_2)$ part of Figure 5. On univariant curve (1), reaction Fo + Cc = A + Do takes place. Tremolite first appears at invariant point (1*) at 485°C, where the assemblage consists of Tr, Fo, Cc, A and Do. A small increase in temperature (but still below 500°C) and a significant increase in $X(CO_2)$ drive the reaction to univariant curve (2), Fo + Tr = A + Do, where at 495°C and $X(CO_2)$ equal to 0.15, talc (Tlc) appears at invariant point (2*). At this point, Tlc coexists with Fo, Tr, A and Do. A subsequent decrease in temperature and $X(CO_2)$ will result in the growth of talc from serpentine and tremolite (A + Tr = Tlc + Do), as shown on univariant curve (3). The above series of reactions may represent a continuum from prograde to retrograde metamorphism, where reactions are driven by internally buffered fluids. Thus univariant curves 1 and 2 [increasing temperature and $X(CO_2)$] represent prograde reactions, and univariant curve 3 [subsequent decrease in T and $X(CO_2)$] represents a retrograde reaction. Although there may have been other paths involved in the crystallization of talc at the Atshan deposit, the above series of reactions is well supported by mineralogical and textural observations.

Model reactions

The Atshan talc deposit had a protracted metamorphic history, and some of the events are recorded in the sequential alteration of the rocks. Reactions were driven by fluids of variable temperature and CO_2:H_2O ratio. On the basis of previously discussed phase relationships, the following sequence of events is suggested for the rocks.

Contact metamorphism

During the initial stage of alteration, dolomite in the impure carbonate beds was partly replaced by forsterite (after Deer *et al.* 1978):

$$\underset{\text{dolomite}}{2CaMg(CO_3)_2} + \underset{\text{quartz}}{SiO_2} \rightarrow \underset{\text{calcite}}{2CaCO_3} + \underset{\text{forsterite}}{Mg_2SiO_4} + 2CO_2 \quad (1A)$$

This reaction was probably associated with the emplacement of the Reiidi grey granite; it occurred above 500°C. In the clastic sedimentary fragments, chlorite was replaced by enstatite, cordierite ± hercynite (after Deer *et al.* 1978):

$$\underset{\text{chlorite}}{(Mg,Fe)_4Al_4Si_2O_{10}(OH)_8} + \underset{\text{quartz}}{5SiO_2} \rightarrow \underset{\text{enstatite}}{2(Mg,Fe)SiO_3} + \underset{\text{cordierite}}{(Mg,Fe)_2Al_4Si_5O_{18}} + 4H_2O \quad (1B)$$

Enstatite–cordierite is a high-temperature (>600°C) assemblage (*cf.* Hoffer & Grant 1980); thus reactions 1A and 1B represent a high-temperature event probably associated with the emplacement of the Reiidi grey granite. Crystallization of the pyroxene hornfels (3010) was probably contemporaneous with reactions 1A and 1B.

Regional metamorphism: re-activation of the faults and shear zones

Below 500°C, forsterite and calcite coexist on the left side of univariant curve 1 (Fig. 5), but will break down to serpentine + dolomite (after Trommsdorff & Evans 1977) with a slight increase in $X(CO_2)$:

$$\underset{\text{forsterite}}{2Mg_2SiO_4} + \underset{\text{calcite}}{CaCO_3} + 2H_2O + CO_2 \rightarrow \underset{\text{serpentine}}{Mg_3Si_2O_5(OH)_4} + \underset{\text{dolomite}}{CaMg(CO_3)_2} \quad (2)$$

With further increase in temperature and $X(CO_2)$ in the fluid, forsterite and tremolite coexist on univariant curve 2, above invariant point 1* (after Trommsdorff & Evans 1977):

$$\underset{\text{tremolite}}{Ca_2Mg_5Si_8O_{22}(OH)_2} + \underset{\text{forsterite}}{18Mg_2SiO_4} + 25\,H_2O + 4CO_2 \rightarrow \underset{\text{serpentine}}{13Mg_3Si_2O_5(OH)_4} + \underset{\text{dolomite}}{2CaMg(CO_3)_2} \quad (3)$$

Univariant curves 2 and 3 represent prograde metamorphism of the carbonate beds. However, a subsequent decrease in temperature and $X(CO_2)$ in the fluid (retrograde reaction) would have resulted in the crystallization of talc at the expense of tremolite and serpentine (after Trommsdorff & Evans 1977):

$$\underset{\text{tremolite}}{2Ca_2Mg_5Si_8O_{22}OH)_2} + \underset{\text{serpentine}}{4Mg_3Si_2O_5(OH)_4} + 8CO_2 \rightarrow$$
$$\underset{\text{talc}}{3Mg_6(Si_8O_{20})(OH)_4} + \underset{\text{dolomite}}{4CaMg(CO_3)_2} + 4H_2O \quad (4)$$

Textural and mineralogical evidence suggests that reactions 1A, 1B and 2–4 represent, at least in part, the metamorphic evolution of the Atshan talc deposit.

Temperature estimates for serpentine and the pyroxenes

The homogenization temperature (T_h) obtained from fluid inclusions in serpentine, 280–310°C, must be corrected for pressure in order to obtain the crystallization temperature (*cf.* Roedder 1982). A pressure estimate for the area is presently unavailable. Thus we will rely on the stability field of serpentine to estimate the maximum temperature of crystallization. The magnetite–serpentine geothermometer of Wenner & Taylor (1974) suggests that lizardite and chrysotile can form at a temperature up to 260°C, and antigorite, up to 450°C. Their results are broadly comparable to thermodynamic calculations of O'Hanley *et al.* (1989) on serpentine stability. Thus, assuming a 2 kbar pressure correction to the values of T_h, the crystallization of serpentine probably occurred at ~450°C. A pressure correction to 3 kbar (yielding a formation temperature of 580°C) would be unacceptable in terms of serpentine stability.

Although relict serpentine is locally present at the Atshan deposit, the variety of mineral assemblages in the mine suggests that the rocks had a complex metamorphic history, including both contact and regional metamorphic events. Serpentine + carbonate + tremolite evidently represents a relatively low-temperature assemblage, whereas enstatite + cordierite + hercynite (granulite), and enstatite + diopside (pyroxene hornfels) represent high-temperature assemblages. It was possible to estimate the temperature of crystallization of the orthopyroxene–clinopyroxene pair by using the two-pyroxene geothermometer of Lindsley (1983). Plotting the composition of enstatite and diopside (Table 1) on the temperature-contoured pyroxene quadrilateral of Lindsley, a minimum temperature in the range 500°–600°C was obtained for the two pyroxenes (at $P < 5$ kbar).

The concentration of Al in tremolite at the Atshan talc deposit is variable, ranging from 0.4 to 5.92 wt.% Al_2O_3 (Table 1). Rice (1977) has observed an increase of Al in tremolite with increasing metamorphic grade in the impure dolomitic limestones in contact with the Boulder batholith, Montana. Unfortunately, we do not have sufficient number of samples to demonstrate whether this "thermometer" could be applied to our suite of rocks to explain the variability in Al concentration in tremolite.

The sulfide–talc association

The association of Mg-rich minerals such as talc and tremolite with sulfides at the Atshan talc mine and at other talc deposits in the Hamata area is enigmatic. However, contrary to the presently favored hypothesis (Hussein *et al.* 1977, Abdel Kader & Shalaby 1982, Rasmy *et al.* 1983), we did not find evidence for VMS-type mineralization. The absence of superimposed potassic and Al-rich alteration zones, and the high concentrations of Mg in rocks of non-igneous origin, would favor a sediment-hosted rather than a volcanogenic origin for the sulfides. The effects of Mg- and K-metasomatism on the host rocks of volcanogenic massive sulfide deposits have been discussed in detail by MacLean & Kranidiotis (1987), and Barrett & MacLean (1991), among others. These authors demonstrated that the addition of large quantities of Mg (from seawater) and K to volcanic rocks should result in zones of pervasive alteration in which chlorite and white mica are dominant. As the addition of chlorite is accompanied by a significant decrease in volume (MacLean & Kranidiotis 1987), such alteration will result in an increase in Al and other major and trace elements. This scenario is the opposite of what has been observed in the trace-element-depleted rocks of the Atshan talc mine, where the low concentrations imply several-fold dilution of the rocks by carbonate or silica-rich material, chert or quartz, for example.

The presence of fractured, fragmented pyrite and pyrrhotite in the clastic sediments suggests that these sulfides were present prior to the high-temperature contact metamorphism. However, the development of pyrite and chalcopyrite rims on hercynite, and of chalcopyrite stringers along cleavages in tremolite, suggests remobilization of some sulfides during the lower-temperature event. Evidently, more work is needed in order to fully characterize and understand the sulfide occurrences at the mine and at other talc occurrences in the Hamata area.

Finally, although contact and regional metamorphism destroyed most primary minerals at the mine, the low and variable concentrations of trace elements, including the *REE*, imply that the protoliths of the Mg-rich rocks were most likely impure carbonate beds containing fragments of clastic sediments. We suggest that the high-temperature assemblages formed at the time of emplacement of the Reiidi grey granite (a quartz diorite body), whereas the subsequent lower-temperature assemblages (including talc) formed during regional metamorphism associated with faulting and shearing. This event would result in enhanced permeability of the rocks, thus, the development of channelways for the

fluids. The abundance of relict serpentine at the mine suggests that the fluids had a relatively high H_2O:CO_2 ratio. Mg was derived from the breakdown of dolomite and possibly magnesite.

Comparison between the Atshan deposit and other carbonate-hosted talc deposits

Talc deposits formed by the hydrothermal alteration of carbonates include the Rabenwald and Lassing deposits in the eastern Alps of Austria, and a talc deposit at Göpfersgrun, Germany, within the Bohemian Massif (Hecht *et al.* 1999). All of the above talc deposits are significantly larger than the Atshan deposit, as their annual production ranges between 20,000 and 110,000 tonnes (Prochaska 1989). The Rabenwald deposit (the largest talc producer in the eastern Alps) occurs within a thrust sheet that was transported over the lower Austroalpine gneisses (Prochaska 1989). The talc orebody at Rabenwald was formed after magnesite, it is intercalated with leucophyllite, and is overlain by mica schists (Prochaska 1989, Moine *et al.* 1989). The Lassing deposit occurs within a strongly tectonized block of the Liesing–Palten lineament, and consists of shallow-water fossiliferous limestones, dolomites, magnesites, and metasediments (Prochaska 1989), and the Göpfersgrun talc deposit occurs within marbles (calcite and dolomite), graphite schists and metasediments. All of the above deposits are metamorphosed to the greenschist facies, and they are associated with shearing, faulting and, in some cases, thrusting (Prochaska 1989, Hecht *et al.* 1999). Mineral assemblages in the deposits consist predominantly of talc, dolomite, magnesite, calcite, and chlorite. Remnants of fossils, organic material and banding (of silicates) are common in the Lassing carbonate beds, and graphite is ubiquitous within magnesite at Rabenwald (Prochaska 1989).

Although the talc orebodies at all four deposits (Rabenwald, Lassing, Göpfelsgrun and Atshan) formed by replacement of carbonates, there are significant differences between the Austrian–German and the Atshan talc deposits: (1) minerals such as serpentine, tremolite, orthopyroxene, clinopyroxene, olivine, cordierite and hercynite are absent from Rabenwald, Lassing and Göpfelsgrun, and (2) fossils are absent from the Atshan orebodies. These differences can be attributed to the initially much higher temperatures of metamorphism at the Atshan mine, to differences in composition (thus, in origin) of the fluid phase, and to differences in the tectonic environments. The Atshan deposit occurs within a thick sequence of arc-related volcanic rocks intercalated with some sediments (*cf.* Abdel-Rahman 1995, Fasfous, 1992) and are intruded by granitic to dioritic rocks, whereas the other three talc deposits occur in tectonized Alpine-type settings within thick carbonate beds and clastic sediments. The Lassing carbonate beds formed in a shallow-water environment (Prochaska 1989), the Rabenwald magnesite represents a "wedge of upper Austroalpine Paleozoic rocks" (Prochaska 1989), and the Göpfersgrun dolomite beds formed in a marine environment (Hecht *et al.* 1999). The only features common to all four deposits are the association of chlorite with talc, the presence of faults and shear zones, and the very low concentration of Fe in the carbonates. This last feature would imply that the carbonates at all four deposits are sedimentary and not hydrothermal in origin (Prochaska 1989).

Conclusions

Our combined mineralogical and geochemical study of the Atshan talc deposit suggests the following:

(1) The low and variable concentrations of Al and trace elements, including the rare-earth elements, in the talc–tremolite-altered rocks are inconsistent with igneous protoliths. The talc deposit most likely formed as replacement of impure siliceous carbonate beds during regional metamorphism, and the source of Mg was the carbonate.

(2) Alteration assemblages at the mine represent at least two metamorphic episodes; pyroxene hornfels and enstatite–cordierite (granulite-grade) assemblages crystallized during contact metamorphism (emplacement of the Reiidi grey granite), whereas the serpentine – tremolite – talc assemblage crystallized during greenschist-facies regional metamorphism associated with faulting and shearing.

(3) The massive talc orebodies crystallized from the breakdown of tremolite, the alteration of serpentine and of forsterite, from fluids (with variable H_2O:CO_2 ratio) expelled along faults and shear zones.

(4) We found no evidence for VMS-type mineralization (and contemporaneous Mg-metasomatism) at the Atshan talc deposit. Thus the small bodies of sulfide possibly represent segregations within the original beds of carbonate-dominant sediment. The presence of late veinlets of chalcopyrite in fragmented, fractured pyrrhotite, sphalerite and pyrite suggests the remobilization (and redistribution) of the metals during the various metamorphic events.

This study has important implications concerning the paragenesis of talc deposits in the Hamata area, Eastern Desert of Egypt. Our study suggests that precursors to the talc orebodies at the Atshan mine were impure carbonate beds. The rocks were subjected to contact metamorphism during the emplacement of the Reiidi grey granite, and later, to regional metamorphism. The origin and extent of carbonate beds in the area are presently unknown. But if all other talc deposits in the Eastern Desert are hosted by rocks of similar composition to those at the Atshan mine, carbonate beds must have been regionally extensive. If this proves to be correct, then a widespread carbonate horizon may have existed in the Eastern Desert prior to igneous activities in the area. Thus using the method described above, the metamorphosed, highly deformed, thrust-faulted and folded

fragments of crust that once were part of the Eastern Desert could all be identified. This would add one more piece to the puzzle in reconstructing the tectonic evolution of the area.

Acknowledgements

We gratefully acknowledge the partial funding of this project by an NSERC research grant to M.P. Gorton, and by the Government of Egypt to Nadia Sharara. N.S. thanks Professors I. Salem and Abou El Eka for their help with the field work. We thank R.F. Martin, A.F.M. Abdel-Rahman and F. Ford for their constructive criticism and helpful suggestions on the first draft of the manuscript. Incorporating their suggestions resulted in a significant improvement of the paper.

References

Abdel Kader, Z. & Shalaby, I.M. (1982): Post-ore alteration at the Atshan talc mine, Hamata, Eastern Desert, Egypt. *Annals Geol. Surv. Egypt* **12**, 163-175.

Abdel-Rahman, A.F.M. (1995): Tectonic-magmatic stages of shield evolution: the Pan African belt in northeastern Egypt. *Tectonophys.* **242**, 223-240.

Ballèvre, M., Hensen, B.J. & Reynard, B. (1997): Orthopyroxene–andalusite symplectites replacing cordierite in granulites from the Strangways Range (Arunta Block, central Australia): a new twist to the pressure–temperature history. *Geology* **25**, 215-218.

Barnes, S.J. & Gorton, M.P. (1984): Trace element analysis by neutron activation with a low flux reactor (SLOWPOKE II): results for international reference rocks. *Geostandards Newsletter* **8**, 17- 23.

Barrett, T.J. & MacLean, W.H. (1991): Chemical, mass and oxygen isotope changes during extreme hydrothermal alteration of an Archean rhyolite, Noranda, Quebec. *Econ. Geol.* **86**, 406-414.

Deer, W.A., Howie, R.A. & Zussman, J. (1978): *An Introduction to the Rock-Forming Minerals.* Longman Group Limited, London, U.K.

El Shazly, M. & Afia, M.S. (1958): Geology of the Umm Samuiki deposits, Eastern Desert, Egypt. *Egyptian J. Geol.* **2**, 25-43.

Engel, A.E.J., Dixon, T.H. & Stern, R.J. (1980): Late Precambrian evolution of Afro-Arabian crust from ocean arc to craton. *Geol. Soc. Am., Bull.* **91**, 699-706.

Fasfous, B.R.B. (1992): Petrochemical and petrogenetic studies on the steatite mineralization of Hamata and Um Omya areas, Eastern Desert, Egypt. *Mans. Sci. Bull.* **19**, 189-212.

_____, Attawiya, M.Y. & El-Rahmani, M. M. (1988): A contribution to the geochemistry of volcanites and associated mineralization in Hamata talc mine, Eastern Desert, Egypt. *J. Afr. Earth Sci.* **7**, 195-199.

Gorton, M.P., Schandl, E.S. & Hoy, T. (1999): Geochemical evolution of the Moyie sills in southeastern British Columbia. *In* Special Volume on the Sullivan SEDEX Deposit, British Columbia (J. Lydon, ed.). *Geol. Surv. Can., Spec. Publ.* (in press).

Greenwood, H.J. (1967): Mineral equilibria in the system $MgO–SiO_2–H_2O–CO_2$. *In* Researches in Geochemistry (P.H. Abelson, ed.). John Wiley and Sons, New York, N.Y. (542-567).

Guiraud, M., Kienast, J.-R. & Rahmani, A. (1996): Petrological study of high-temperature granulites from In Ouzzal, Algeria: some implications on the phase relationships in the FMASTOCr system. *Eur. J. Mineral.* **8**, 1375-1390.

Harris, N.B.W. & Holland, T.J.B. (1984): The significance of cordierite–hypersthene assemblages from the Beitbridge region of the central Limpopo Belt; evidence for rapid decompression in the Archean? *Am. Mineral.* **69**, 1036-1049.

Hecht, L., Freiberger, R., Gilg, H.A., Grundmann, G. & Kostitsyn, Y.A. (1999): Rare earth element and isotope (C, O, Sr) characteristics of hydrothermal carbonates: genetic implications for dolomite-hosted talc mineralization at Göpfersgrun (Fichtelgebirge, Germany). *Chem. Geol.* **155**, 115-130.

Hoffer, E. & Grant, J.A. (1980): Experimental investigation of the formation of cordierite–orthopyroxene parageneses in pelitic rocks. *Contrib. Mineral. Petrol.* **73**, 15-22.

Hume, W.F. (1937): *Geology of Egypt.* **2**(III). *The Minerals of Economic Value.* Geological Survey of Egypt, Cairo, Egypt.

Hussein, A.A.A. & El Sharkawi, M.A. (1990): Mineral deposits. *In* The Geology of Egypt (R. Said, ed.). A.A. Balkema, Rotterdam, The Netherlands (511-566).

Johannes, W. (1969): An experimental investigation of the system $MgO–SiO_2–H_2O–CO_2$. *Am. J. Sci.* **267**, 1083-1104.

Kovacik, J. (1961): Report on geological prospecting of Cu, Zn, Pb at Umm Samiuki Eastern Desert, Egypt. Internal Rep., Geol. Surv. Egypt (prepared by Polytechnical Foreign Trade Cooperation, Prague, Czech Republic).

Kretz, R. (1983): Symbols for rock-forming minerals. *Am. Mineral.* **68**, 277-279.

Lindsley, D.H. (1983): Pyroxene thermometry. *Am. Mineral.* **68**, 477-493.

MacLean, W.H. & Kranidiotis, P. (1987): Immobile elements as monitors of mass transfer in hydrothermal alteration: Phelps Dodge massive sulfide deposit, Matagami, Quebec. *Econ. Geol.* **82**, 951-962.

Mansour, M.S., El Masry, S., El-Danaf, M.A. & El-Sayed, N.B. (1962): Report on the prospecting activities for

Cu–Zn deposits in Umm Samiuki and Darhib region, Internal Rep., Geol. Surv. of Egypt, Cairo, Egypt.

MOINE, B., FORTUNÉ, J.P., MOREAU, P. & VIGUIER, F. (1989): Comparative mineralogy, geochemistry and conditions of the formation of two metasomatic talc and chlorite deposits: Trimouns (Pyrenées, France) and Rabenwald (eastern Alps, Austria). *Econ. Geol.* **84**, 1398-1416.

NESSIM, S., AFIA, M.S., FAHIM, M. & FODA, A.A. (1954): Report on the prospecting work carried out in Wadi Hamata area, South Eastern Desert, Department of Mines and Quarries, Mineral Research Section, Geol. Surv. of Egypt, Cairo, Egypt.

O'HANLEY, D.S., CHERNOSKY, J.V., JR. & WICKS, F.J. (1989): The stability of lizardite and chrysotile. *Can. Mineral.* **27**, 483-493.

PEARCE, J.A. (1983): Role of the sub-continental lithosphere in magma genesis at active continental margins. *In* Continental Basalts and Mantle Xenoliths (C.J. Hawkesworth & M.J. Norry, eds.). Shiva Press, Cheshire, U.K. (230-249).

PROCHASKA, W. (1989): Geochemistry and genesis of Austrian talc deposits. *Appl. Geochem.* **4**, 511- 525.

RASMY, A.H., TAKLA, M.A. & GAD, M.A. (1983): Alteration associated with ore formation at Umm Samiuki, South Eastern Desert, Egypt. *Annals Geol. Surv. Egypt* **13**, 1-21.

RICE, J.M. (1977): Contact metamorphism of impure dolomitic limestone in the Boulder aureole, Montana. *Contrib. Mineral. Petrol.* **59**, 237-259.

ROEDDER, E. (1982): Origin of fluid inclusions and changes that occur after trapping. *In* Fluid Inclusions: Applications to Petrology. *Mineral. Assoc. Can., Short-Course Handbook* **6**, 101-137.

SCHANDL, E.S. (1989): *Talc–Carbonate Alteration of Ultramafic Rocks in the Kidd Volcanic Complex, the Slade Forbes and Munro Asbestos Deposits in the Abitibi Greenstone Belt, Timmins, Ontario.* Ph.D. thesis, Univ. of Toronto, Toronto, Ontario.

_____, GORTON, M.P. & BLEEKER, W. (1999): A systematic study of rare earth and trace element geochemistry of host rocks to the Kidd Creek volcanogenic massive sulfide deposit. *Econ. Geol., Monogr.* **10** (in press).

_____, _____ & WASTENEYS, H.A. (1995): Rare earth element geochemistry of the metamorphosed volcanogenic massive sulfide deposits of the Manitouwadge mining camp, Superior Province, Canada: a potential exploration tool? *Econ. Geol.* **90**, 1217-1236.

_____ & NALDRETT, A.J. (1992): CO_2 metasomatism of serpentinites, south of Timmins, Ontario. *Can. Mineral.* **30**, 93-108.

_____ & WICKS, F.J. (1991): Two stages of CO_2 metasomatism at the Munro mine, Munro Township, Ontario: evidence from fluid inclusion, stable isotope, and mineralogical studies. *Can. J. Earth Sci.* **28**, 721-728.

_____ & _____ (1993): Carbonate and associated alteration of ultramafic and rhyolitic rocks at the Hemingway property, Kidd Creek volcanic complex, Timmins, Ontario. *Econ. Geol.* **88**, 1615- 1635.

SEARLE, D.L., CARTER, G.S. & SHALABY, I.M. (1976): Mineral exploration at Umm Samiuki. *U.N. Tech. Rep.* **Egypt 72-008/3**.

SKIPPEN, G. (1974): An experimental model for low pressure metamorphism of siliceous dolomitic marble. *Am. J. Sci.* **274**, 487-509.

STIX, J. & GORTON, M.P. (1992): Trace element analyses of ten U.S. Geological Survey standards by neutron activation analysis, using a low flux reactor. *Geostandards Newsletter* **16**, 21-26.

TROMMSDORFF, V. & EVANS, B.W. (1977): Antigorite-ophicarbonates: phase relations in a portion of the system $CaO–MgO–SiO_2–H_2O–CO_2$. *Contrib. Mineral. Petrol.* **60**, 39-56.

VAIL, J.R. (1985): Pan-African (late Precambrian) tectonic terrains and the reconstruction of the Arabian–Nubian Shield. *Geology* **13**, 839-842.

WENNER, D.B. & TAYLOR, H.P., JR. (1974): D/H and $^{18}O/^{16}O$ studies of serpentinization of ultramafic rocks. *Geochim. Cosmochim. Acta* **38**, 1255-1286.

ZIDAN, B.I. (1989): Mineralogy and origin of the Precambrian massive sulphide deposit, Atshan area, Egypt. First Conference of Geochemistry, Alexandria University, Alexandria, Egypt (238-251).

Received November 15, 1998, revised manuscript accepted July 31, 1999.

Appendix: Mineral Assemblages in Individual Samples at the Atshan Talc Deposit, Hamata Area, Egypt

ASH–A: Tr, Tlc, Srp [the symbols are those of Kretz (1983), except that Mgt stands for magnetite).
ASH–B: Opx, Crd, Hc, Tlc, Tr, Srp, Ap
ASH–C: Opx, Crd, Tlc, Phl, Hc, Fo, Srp, Rt, Ap
ASH–D: Chl, Mgt, Ilm, Ap
ASH–E: Dol, Srp
3001: Opx, Crd, Tlc, Hc, Dol, Phl, Chl, Ccp, Po, Ap
3002: Tlc, Srp, Tr, Dol, Py, Sp
3003: Tlc, Srp, Tr, Chl
3004: Tr, Tlc, Srp, Dol
3006: Tlc, Srp, Tr, Sp
3007: Srp, Dol, Chl
3008: Amp, Pl, Tlc, Qtz, Chl, Mgt
3009: (Ab + Qtz), Tr, Tlc, Dol. Cal, Chl
3010: Opx, Cpx, Ol, Srp, Tlc, Tr, Chl, Sp
3011: Srp, Dol, Tlc
3012: Dol, Srp, Ap
3013: Ab, Act, Qtz, Tlc
3014: Tr, Tlc, Dol, Srp
3015: Tr, Tlc, Srp, Dol